Article:

Shen, J.X., Zhu, Z.Q. and Howe, D. (2004) Sensorless flux-weakening control of permanent-magnet brushless machines using third harmonic back EMF. IEEE Transactions on Industry Applications, 40 (6). pp. 1629-1636. ISSN 0093-9994

https://doi.org/10.1109/TIA.2004.836157

Sensorless Flux-Weakening Control of Permanent-Magnet Brushless Machines Using Third Harmonic Back EMF

J. X. Shen, *Senior Member, IEEE*, Z. Q. Zhu, *Senior Member, IEEE*, and David Howe

***Abstract*—The sensorless control of brushless machines by detecting the third harmonic back electromotive force is a relatively simple and potentially low-cost technique. However, its application has been reported only for brushless dc motors operating under normal commutation. In this paper, the utility of the method for the sensorless control of both brushless dc and ac motors, including operation in the flux-weakening mode, is demonstrated.**

***Index Terms*—Back electromotive force (EMF), brushless drives, permanent-magnet machines, sensorless control.**

I. INTRODUCTION

NUMEROUS sensorless control techniques have been developed for brushless dc (BLDC) and brushless ac (BLAC) machines. For example, methods based on the detection of the zero crossing of the back-electromotive-force (EMF) waveforms [1], [2] are simple, and various commercial ICs are available for BLDC drives. However, they are not applicable to BLAC operation, or even to BLDC operation if the commutation advance or the current decay in the freewheeling diodes is greater than 30° electrical, since the zero crossing of the back EMFs cannot then be detected. Theoretically, back-EMF reconstruction and integration methods [3] are suitable for surface-mounted permanent-magnet (SPM) BLDC and BLAC motors, but not for interior permanent-magnet (IPM) motors, since the stator winding inductance is simulated by a transformer or appropriate electronic components, and cannot vary with rotor position. Moreover, the hardware is relatively complex and implementation is difficult. In all back-EMF-based sensorless techniques, the low-speed performance is limited, and an open-loop starting strategy is required [1]–[3]. In most other sensorless control strategies, such as flux observers [4], model-reference adaptive control [5], [6], extended Kalman filters [7], and adaptive sliding observers [8], a mathematical model of the machine is required. Further, phase or terminal voltages often have to be measured and A/D converters are required. In order to reduce the number of voltage transducers, voltages can be deduced from the inverter switching status and the measured dc-link voltage [9]. Rotor saliency detection methods [10]–[12] are suitable for low-speed operation, and applicable to IPM BLDC and BLAC drives. Methods which utilize the third harmonic component of the back EMF are attractive since they are relatively simple and potentially low cost. To date, however, their performance has been reported only for BLDC motors operating under normal commutation, i.e., without commutation advance or flux weakening [3], [13]. In this paper, the utility of the third harmonic back-EMF method is demonstrated for the sensorless operation of both BLDC and BLAC drives.

Three methods have been proposed to extract the third harmonic component of the back EMF [3], [13]–[15]. These are evaluated and the most appropriate is identified and implemented for the sensorless control of both BLDC and BLAC drives, including operation in the flux-weakening mode. Finally, experimental results are given to further verify the utility of the method.

Paper IPCSD-04-061, presented at the 2003 IEEE International Electric Machines and Drives Conference, Madison, WI, June 1–4, and approved for publication in the IEEE TRANSACTIONS ON INDUSTRY APPLICATIONS by the Industrial Drives Committee of the IEEE Industry Applications Society. Manuscript submitted for review September 12, 2003 and released for publication August 5, 2004.

J. X. Shen was with the Department of Electronic and Electrical Engineering, University of Sheffield, Sheffield S1 3JD, U.K. He is now with the College of Electrical Engineering, Zhejiang University, Hangzhou 310027, China (e-mail: j.x.shen@ieee.org).

Z. Q. Zhu and D. Howe are with the Department of Electronic and Electrical Engineering, University of Sheffield, Sheffield S1 3JD, U.K. (e-mail: z.q.zhu@ieee.org; d.howe@shef.ac.uk).

Digital Object Identifier 10.1109/TIA.2004.836157

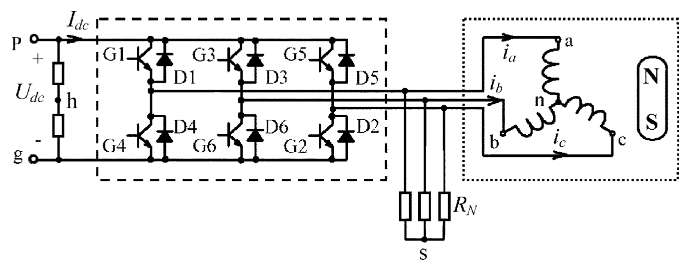

Fig. 1. Schematic of brushless motor with Y-connected resistors.

II. EVALUATION OF METHODS FOR EXTRACTING THIRD HAMONIC BACK EMF

Fig. 1 shows a schematic of a permanent-magnet brushless drive with Y-connected resistors to enable the third harmonic component of the back EMF to be sensed. In the literature, three methods for obtaining the third harmonic voltage have been proposed: 1) from the voltage u_{sn} between the star point "s" of the resistor network and the neutral point "n" of the stator windings [3], [13], [14]; 2) from the voltage u_{sh} between "s" and the midpoint "h" of the dc bus [13]; and 3) from the voltage u_{nh} between "n" and "h" [15]. These are evaluated in detail as follows.

A. Voltage u_{sn}

Assuming the inductances of the brushless motor are constant and that the three phases are symmetrical, from Fig. 1

$$u_{sn} = \frac{(u_{an} + u_{bn} + u_{cn})}{3} = (e_3 + e_9 + e_{15} + \cdots) \approx e_3 = -E_{m3} \sin 3\theta_r \quad (1)$$

where e_3, e_9, and e_{15} are the triplen harmonics of the back EMF. Since the derivation does not depend on the motor operating mode, the third harmonic back EMF can be extracted from the voltage u_{sn} irrespective of whether the motor is operated in BLDC or BLAC mode, provided, of course, that the phase back-EMF waveform contains a third harmonic component. Fig. 2 shows measured waveforms of u_{sn} when a surface-mounted magnet motor was run as BLAC with pulsewidth modulation (PWM), and as a BLDC motor both with and without PWM. Although, theoretically, u_{sn} should have a smooth and clean waveform, as will be seen, in practice high-frequency noise exists as a result of commutation and PWM switching events. However, this can be easily eliminated by using either a low-pass filter (LPF) or a bandpass filter (BPF).

B. Voltage u_{sh}

From Fig. 1

$$u_{sh} = \frac{(u_{ag} + u_{bg} + u_{cg})}{3} - \frac{U_{\mathrm{dc}}}{2}. \quad (2)$$

In BLAC mode, the terminal voltages (u_{ag}, u_{bg}, and u_{cg}) are either 0 or U_{dc}. Therefore, the voltage u_{sh} comprises a series of pulses, the amplitude being either $U_{\mathrm{dc}}/2$ or $U_{\mathrm{dc}}/6$, as shown in Fig. 3. Clearly, u_{sh} cannot be used for the sensorless control of a BLAC drive.

In BLDC mode without PWM

$$u_{sh} = \frac{e_k}{2} - \frac{(e_a + e_b + e_c)}{6} \quad (3)$$

where the subscript k represents the nonenergized phase. It was assumed in [13] that the back-EMF waveforms of the two energized phases were identical and instantaneously sum to zero. Thus, (3) was rewritten as

$$u_{sh} = \frac{(e_a + e_b + e_c)}{2} - \frac{(e_a + e_b + e_c)}{6} = e_3 + e_9 + e_{15} + \cdots \approx e_3. \quad (4)$$

It would appear, therefore, that the third harmonic component of the back EMF could be extracted from u_{sh}. However, this assumption is only valid when the back-EMF waveform is trapezoidal with a flat top $= 120^\circ$ electrical, which is not generally the case in practice. In general, (3) can be further derived as

$$u_{sh} = \frac{e_k}{2} - \frac{(e_3 + e_9 + e_{15} + \cdots)}{2} = \frac{(e_{k1} + e_{k5} + e_{k7} + e_{k11} + \cdots)}{2} \approx \frac{e_{k1}}{2}. \quad (5)$$

Clearly, u_{sh} contains information on nonzero-sequence components in the back EMF of the nonenergized phase. Moreover, if the current in the freewheeling diode has not decayed to zero or if PWM is employed, pulse or noise is introduced in u_{sh}, as evidenced in Fig. 3. Therefore, in general, it is inappropriate to use u_{sh} for the sensorless control of a BLDC drive.

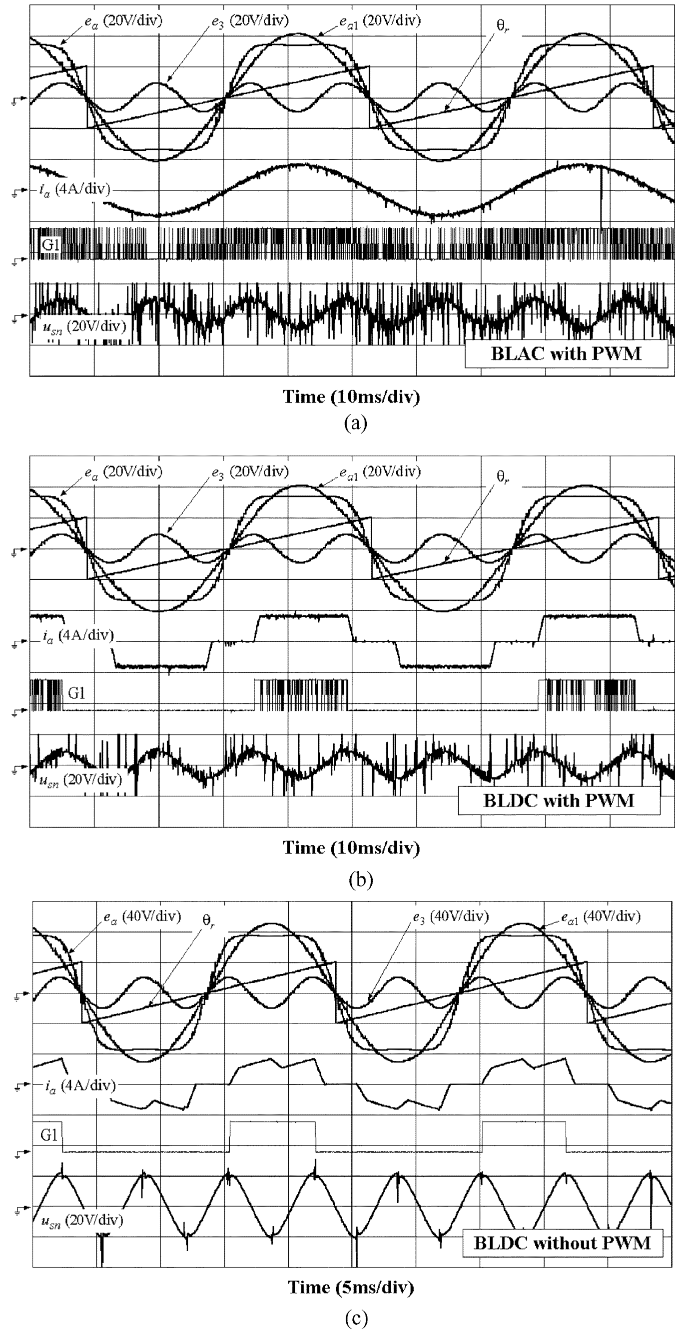

Fig. 2. Measured waveforms of $u_{sn}(U_{\mathrm{dc}} = 200$ V). θ_r: measured rotor position; e_a, e_{a1}, e_3: predicted phase back EMF and its fundamental and third harmonic components, which are predicted according to θ_r and EMF constant for each harmonic; i_a: measured phase current; G1: measured gate drive signal. (a) BLAC operation with PWM. (b) BLDC operation with PWM. (c) BLDC operation without PWM.

C. Voltage u_{nh}

From Fig. 1

$$u_{nh} = u_{sh} - u_{sn}. \quad (6)$$

In BLAC mode, u_{sh} is essentially noise while u_{sn} represents the zero-sequence back EMF of a nonenergized phase. Therefore, while u_{nh} contains the third harmonic component of

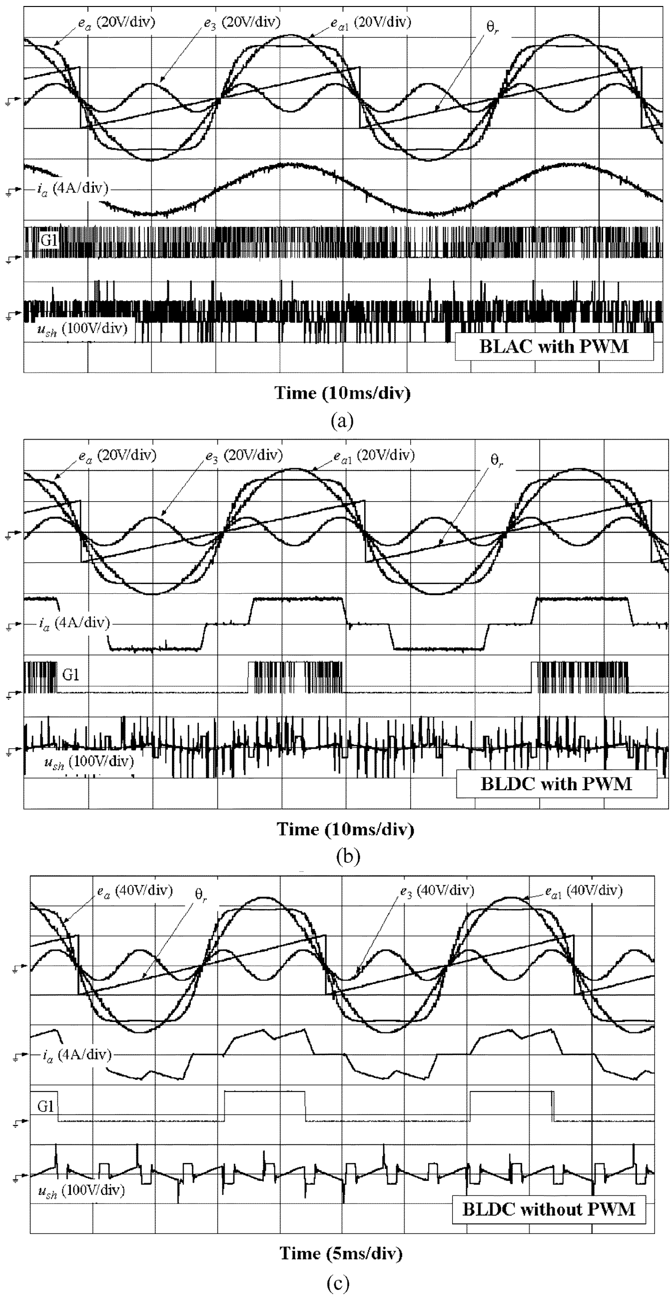

Fig. 3. Measured waveforms of $u_{sh}(U_{\mathrm{dc}} = 200\ \mathrm{V})$. (a) BLAC operation with PWM. (b) BLDC operation with PWM. (c) BLDC operation without PWM.

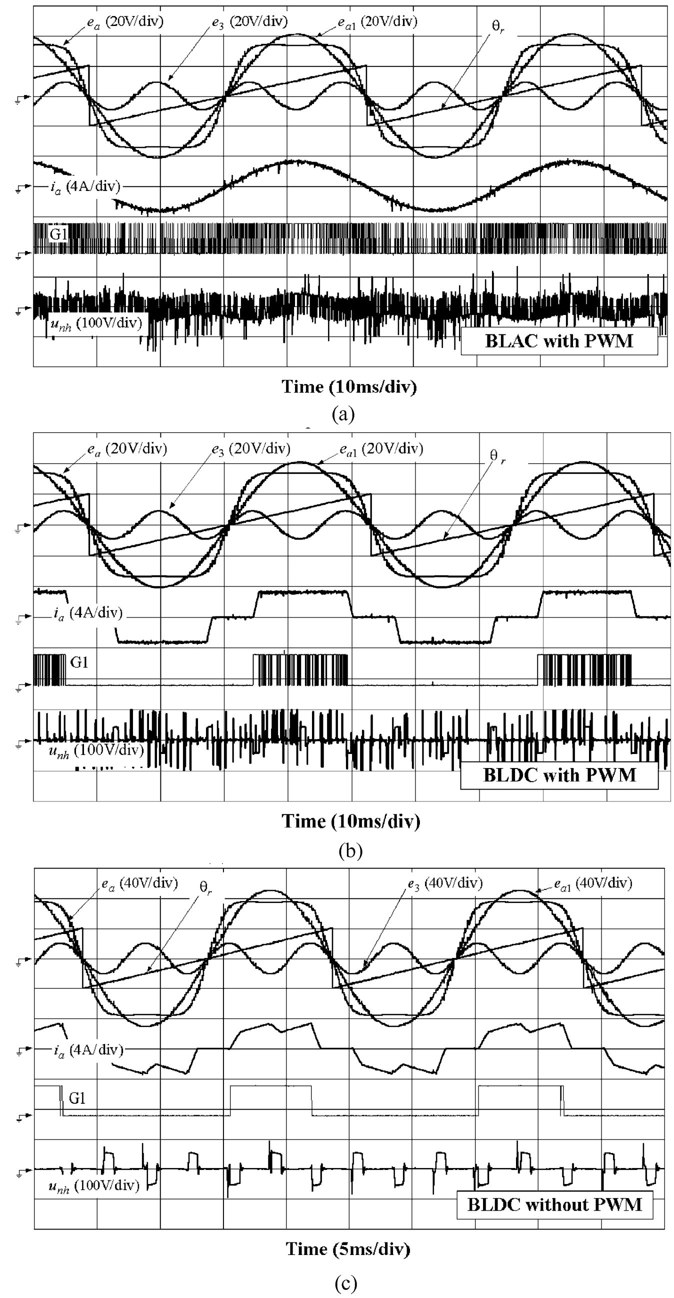

Fig. 4. Measured waveforms of $u_{nh}(U_{\mathrm{dc}} = 200\ \mathrm{V})$. (a) BLAC operation with PWM. (b) BLDC operation with PWM. (c) BLDC operation without PWM.

back EMF, it also contains significant noise, as shown in Fig. 4. Clearly, it is more difficult to extract the third harmonic component of back EMF from u_{nh} than from u_{sn}. Moreover, both methods require access to the winding neutral point.

In BLDC mode, u_{nh} can be derived by substituting (1) and (5) into (6), to give

$$\begin{aligned} u_{nh} &= \frac{[e_k - (e_3 + e_9 + \cdots)]}{2} - (e_3 + e_9 + \cdots) \\ &= \frac{e_k}{2} - \frac{3(e_3 + e_9 + \cdots)}{2} \\ &= \frac{e_k}{2} - \frac{(e_a + e_b + e_c)}{2} \\ &= -\frac{(e_m + e_n)}{2} \end{aligned} \tag{7}$$

where the subscripts m and n represent two energized phases. Clearly, u_{nh} does not contain any effective information that can be used to deduce the rotor position. Moreover, if the phase back EMF has an ideal trapezoidal waveform, the instantaneous sum of the back EMFs of the energized phases is effectively zero, as shown in Fig. 4, the waveform of u_{nh} comprising pulses due to current decaying in the freewheeling diodes and noise due to PWM switching.

From the foregoing, only the voltage u_{sn} is suitable for the third harmonic back-EMF sensorless operation of both BLDC and BLAC SPM motors, as summarized in Table I. Therefore, although it requires access to the neutral point of the stator winding, u_{sn} can be used for sensorless control in both the constant-torque and flux-weakening modes.

TABLE I
SUMMARY OF ALTERNATIVE SENSING METHODS

Voltage	BLDC mode	BLAC mode
u_{sn}	3rd-harmonic emf	3rd-harmonic emf
u_{sh}	50% of fundamental phase emf + PWM noise + distortion due to free-wheel diode conduction	PWM noise
u_{nh}	sum of fundamental phase emfs in 2 energised phases + PWM noise + distortion due to free-wheel diode conduction	3rd-harmonic emf + PWM noise

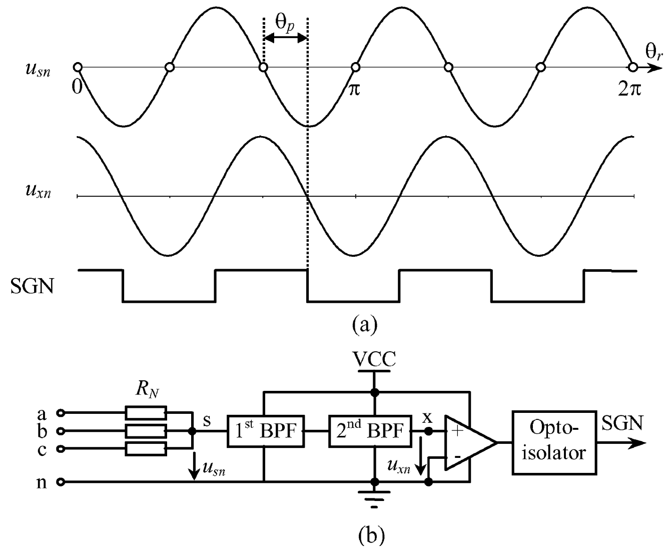

Fig. 5. Zero-crossing detection of third harmonic voltage. (a) Typical waveforms. (b) Detection hardware.

III. SENSORLESS OPERATION: NONFLUX-WEAKENING MODE

A. Rotor Position Estimation

The zero crossings in the third harmonic voltage u_{sn} correspond to rotor positions $0, \pi/3, 2\pi/3, \ldots, 2\pi$ rad., respectively, as illustrated in Fig. 5(a). Generally, other zero-sequence EMF harmonics in SPM motors will be relatively small, as is the case for the experimental motor, for which details are given in the Appendix. In practice, however, u_{sn} will contain noise due to switching events and asymmetries between phases. Therefore, a BPF is employed before the zero crossings of the third harmonic voltage u_{xn} are detected, as illustrated in Fig. 5. Since the operating speed range of the experimental six-pole motor varies from 150 to 1600 r/min, the frequency of third harmonic EMF varies from 22.5 to 240 Hz. Hence, the low and high cutoff frequencies of the BPF were chosen to be 2.2 Hz and 2.4 kHz, which are an order of magnitude different to the minimum and maximum frequencies. u_{xn} is then processed with a voltage comparator and opto-isolator to generate a digital signal SGN. The BPF introduces a phase delay θ_p between u_{sn} and u_{xn}, as illustrated in Figs. 5(a) and 6, which can be calculated from the filter parameters and the motor speed ω_{rm}, ω_{rm} being obtained from the frequency of SGN.

Sensorless control has been implemented with a TMS320C31 digital signal processor (DSP), the rotor position being estimated at time increments $\Delta t_c = 50$ μs, as set by the DSP timer, the flowchart of the timer interrupt service routine (ISR) being shown in Fig. 7. The DSP scans the signal SGN in the timer ISR. If a falling edge is detected, the estimated rotor position θ_{re} is updated incrementally by either θ_p, $(2\pi/3 + \theta_p)$ or $(4\pi/3 + \theta_p)$. For example, if the updated value on the occurrence of the last falling edge was θ_p, the updated value should be $(2\pi/3 + \theta_p)$, while the next will be $(4\pi/3 + \theta_p)$, and so on. In order to avoid erroneous updating, two requirements have to be satisfied: 1) noise in the signal SGN must be distinguishable and 2) the first update of θ_{re} must be correct. Details of how to achieve these requirements are given in the following sections. The rising edge of SGN could be similarly utilized to enable θ_{re} and, therefore, ω_{rm}, to be updated six times per electrical cycle. However, in order to simplify the software, updating is implemented only three times each cycle, viz., on SGN falling edges, since no discernible performance deterioration was observed. If a falling edge is not detected during the execution of the DSP timer ISR, the rotor position is simply estimated by integration of the motor speed, i.e.,

$$\theta_{re(K)} = \theta_{re(K-1)} + \omega_{rm} \cdot \Delta t_c. \tag{8}$$

Once the rotor position has been estimated, the instantaneous current in the windings can be controlled to facilitate either BLAC or BLDC operation, and this is also implemented in the

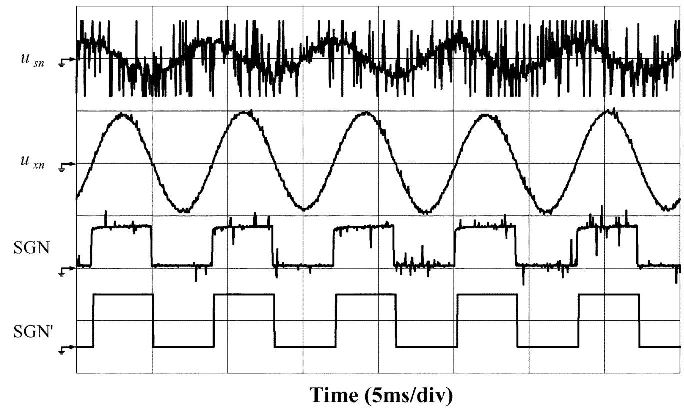

Fig. 6. u_{sn}, u_{xn}, and detection circuit output signal, without (SGN) and with (SGN') noise suppression, measured at 200 Vdc, 2.86 Adc, 829 r/min, BLAC operation with PWM and without flux-weakening (u_{sn}: 50 V/div; u_{xn}, SGN, SGN': 5 V/div).

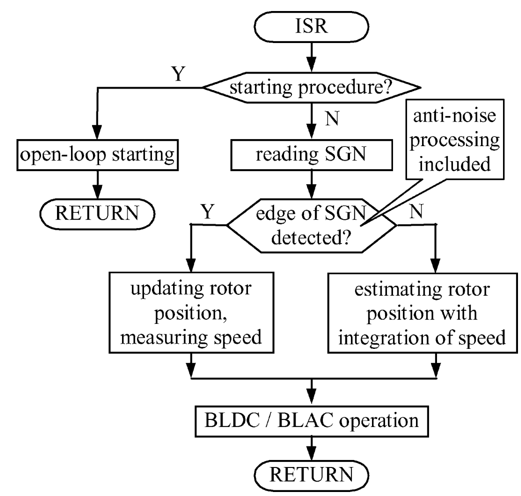

Fig. 7. DSP timer interrupt service routine for sensorless control.

TABLE II
BLDC CURRENTS

$(\theta_{re}+\theta_{ad})$	0~ π/6	π/6~ π/2	π/2~ 5π/6	5π/6~ 7π/6	7π/6~ 3π/2	3π/2~ 11π/6	11π/6 ~2π
$\tilde{i}_a$	0	$-\tilde{I}_m$	$-\tilde{I}_m$	0	$\tilde{I}_m$	$\tilde{I}_m$	0
$\tilde{i}_b$	$\tilde{I}_m$	$\tilde{I}_m$	0	$-\tilde{I}_m$	$-\tilde{I}_m$	0	$\tilde{I}_m$
$\tilde{i}_c$	$-\tilde{I}_m$	0	$\tilde{I}_m$	$\tilde{I}_m$	0	$-\tilde{I}_m$	$-\tilde{I}_m$

DSP timer ISR. By way of example, the phase currents for BLAC operation are

$$\begin{cases} \tilde{i}_a = -\tilde{I}_m \sin(\theta_{re} + \theta_{ad}) \\ \tilde{i}_b = -\tilde{I}_m \sin\left(\theta_{re} + \theta_{ad} - \frac{2\pi}{3}\right) \\ \tilde{i}_c = -\tilde{I}_m \sin\left(\theta_{re} + \theta_{ad} + \frac{2\pi}{3}\right) \\ \tilde{I}_m = \sqrt{\tilde{i}_d^2 + \tilde{i}_q^2} \\ \theta_{ad} = \arctan\left(-\frac{\tilde{i}_d}{\tilde{i}_q}\right) \end{cases} \tag{9}$$

while those for BLDC operation are specified in Table II, where θ_{ad} is the commutation-advance angle.

B. Noise Suppression

In a practical system, the digital signal SGN may contain noise which could cause an erroneous update of the estimated rotor position. Hence, signal edges which may arise due to noise must be distinguishable from true falling edges using the DSP software. Therefore, the values of SGN in three successive timer interrupts are recorded and compared. Only if they are identical is their value accepted as the actual value of SGN. Usually, the duration of the noise is much less than Δt_c, experimental results showing that it usually ranges from $10 \sim 20\,\mu$s. Practically, such noise is highly unlikely to occur three times in succession within a constant time interval of $\Delta t_c = 50\,\mu$s. Therefore, noise can generally be recognized and discarded. However the foregoing procedure results in an actual falling edge in SGN being confirmed after it occurs, the time delay varying from $2\Delta t_c$ to $3\Delta t_c$, i.e., the average delay is $2.5\Delta t_c$. The equivalent phase delay θ_d can be calculated from the motor speed, and while it may be negligible at low speed, it may be considerable at high speed. Therefore, θ_p in the previously described rotor position update procedure should be replaced by $(\theta_p + \theta_d)$. On the other hand, the additional time delay which is caused by noise processing has little influence on the estimated speed measurement, as its variation is much shorter than the cycle time of SGN.

The number of recorded and compared values of SGN is determined experimentally according to the nature of the noise, more values being required as the noise becomes more prominent. In a practical system, however, the noise is effectively eliminated by this noise processing procedure when the average of three readings is used, as shown in Fig. 7, which compares the signal of SGN with and without noise suppression.

IV. SENSORLESS OPERATION: FLUX-WEAKENING MODE

The effectiveness of third harmonic back-EMF sensorless control has been demonstrated on the experimental motor for which details are given in the Appendix and whose base speed is 830 r/min. As will be seen from Figs. 2–4, the phase back-EMF waveform is not a pure sine wave. It contains a sufficiently high third harmonic component to facilitate implementation of the proposed sensorless control strategy in both BLDC and BLAC modes. However, in order to achieve the same rated torque, the amplitude of the phase current reference for BLDC operation is set to 3.30 A while that for BLAC operation is set to 3.56 A.

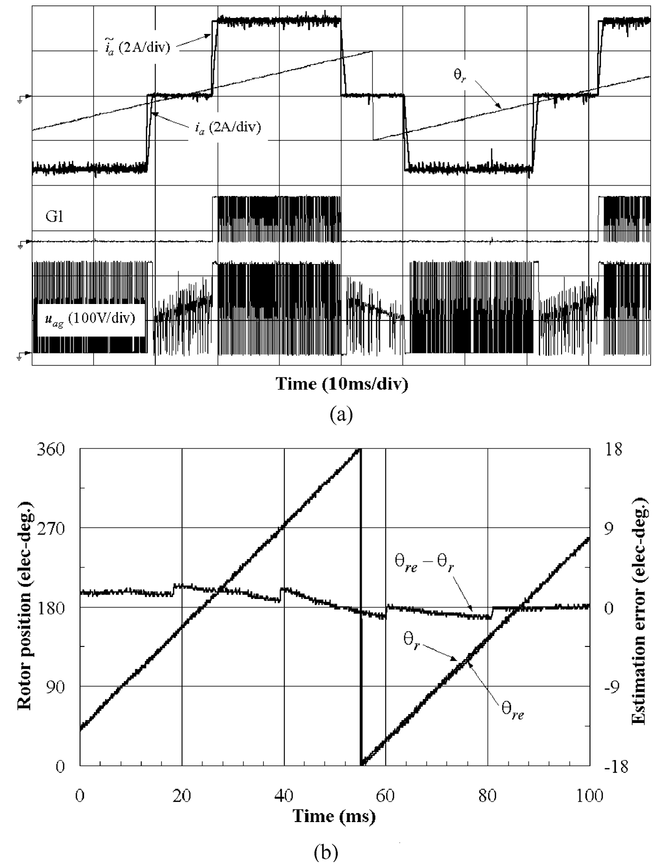

Fig. 8. BLDC operation without commutation advance ($U_{\rm dc} = 200$ V, 320 r/min, 4.62 N·m). $\tilde{i}_a$: current reference; i_a: actual current; G1: gate drive signal; u_{ag}: terminal voltage; θ_r: actual rotor position; θ_{re}: estimated rotor position; θ_{re}–θ_r: position estimation error. (a) Measured waveforms. (b) Rotor position and error.

A. Flux-Weakening in BLDC Mode

Below base speed, the phase current is in phase with the back EMF, and the current amplitude is PWM regulated to produce rated output torque, as shown in Fig. 8. Above base speed, commutation is progressively advanced, so as to achieve flux weakening, until the phase current waveforms ultimately become continuous, as shown in Fig. 9. Clearly, when θ_{ad} is $> 30^\circ$ or the current waveforms are almost continuous, the zero crossing of the back EMF in a nonenergized phase is not discernable in the terminal voltage [16], and conventional sensorless operation based on detection of the zero crossings of the phase back-EMF waveforms [1], [2] is not possible. However, the proposed third harmonic back-EMF sensorless method results in high accuracy, as can be seen by comparing the measured and estimated rotor positions, and observing the estimated rotor position error.

The torque which can be realized in the flux-weakening mode depends on the commutation-advance angle θ_{ad}, as shown by

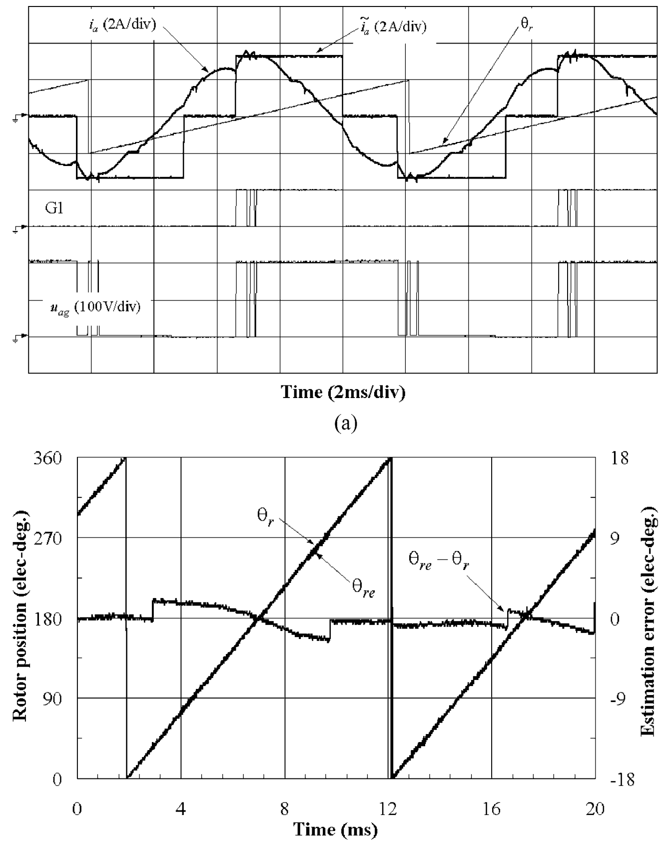

Fig. 9. BLDC operation with 45° commutation advance ($U_{\rm dc} = 200$ V, 1950 r/min, 0.25 N·m). (a) Measured waveforms. (b) Rotor position and error.

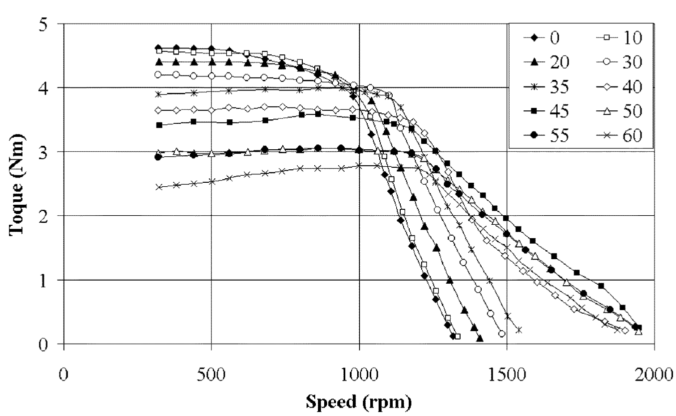

Fig. 10. Torque–speed curves of BLDC machine with different commutation-advance angles θ_{ad}.

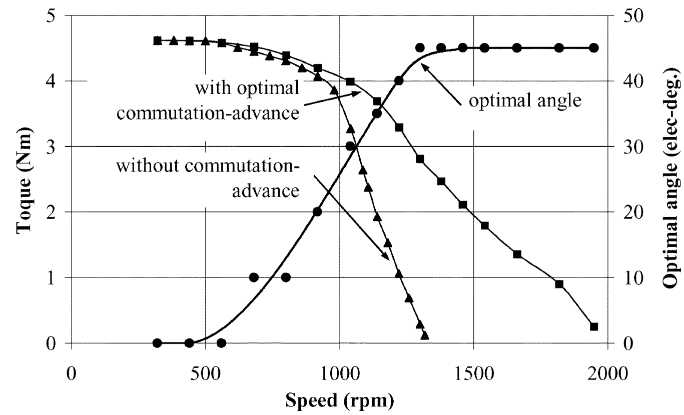

Fig. 11. Torque–speed characteristics of BLDC machine with and without commutation advance, and optimal commutation-advance angle θ_{ad}.

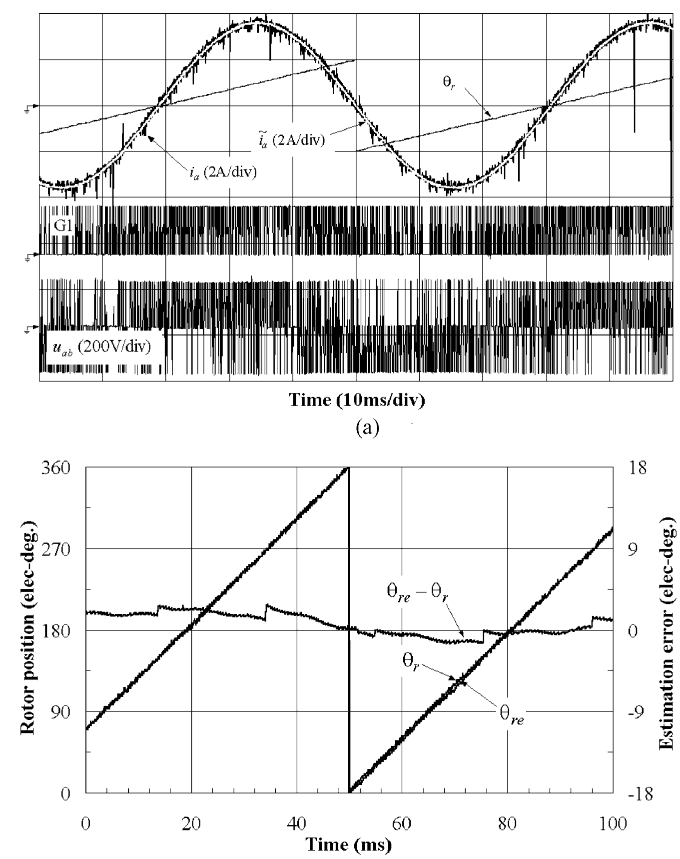

Fig. 12. BLAC operation without flux weakening ($U_{\rm dc} = 200$ V, 320 r/min, 4.63 N·m). $\tilde{i}_a$: current reference; i_a: actual current; G1: gate drive signal; u_{ab}: line-to-line voltage; θ_r: actual rotor position; θ_{re}: estimated rotor position; θ_{re}–θ_r: position estimation error. (a) Measured waveforms. (b) Rotor position and error.

the experimental results in Fig. 10. The optimal values of θ_{ad} for maximum torque at any speed can be deduced from such data, as shown in Fig. 11, which compares the torque–speed characteristics which result both with and without optimal commutation advance.

B. Flux Weakening in BLAC Mode

In order to maximize the output power above the base speed the windings must be supplied with the optimum value of negative d-axis current [17], [18]. With the amplitude of the current and voltage vectors set at the maximum values, $I_{\max}$ and $U_{\max}$, the d-axis current reference is calculated, with due account of the winding resistance voltage drop ($RI_{\max}$), from [17]

$$\tilde{i}_d = \frac{(U_{\max} - RI_{\max})^2}{2\omega^2 (L-M)\Psi_f} - \frac{[(L-M)I_{\max}]^2 + {\Psi_f}^2}{2(L-M)\Psi_f} \tag{10}$$

where Ψ_f is the permanent-magnet excitation flux linkage, and $U_{\max}$ is usually set at $2U_{\rm dc}/\pi$ [17]. $\tilde{i}_d$ is set to 0 if the calculated value is > 0, or set to $-I_{\max}$ if the calculated value is $<$

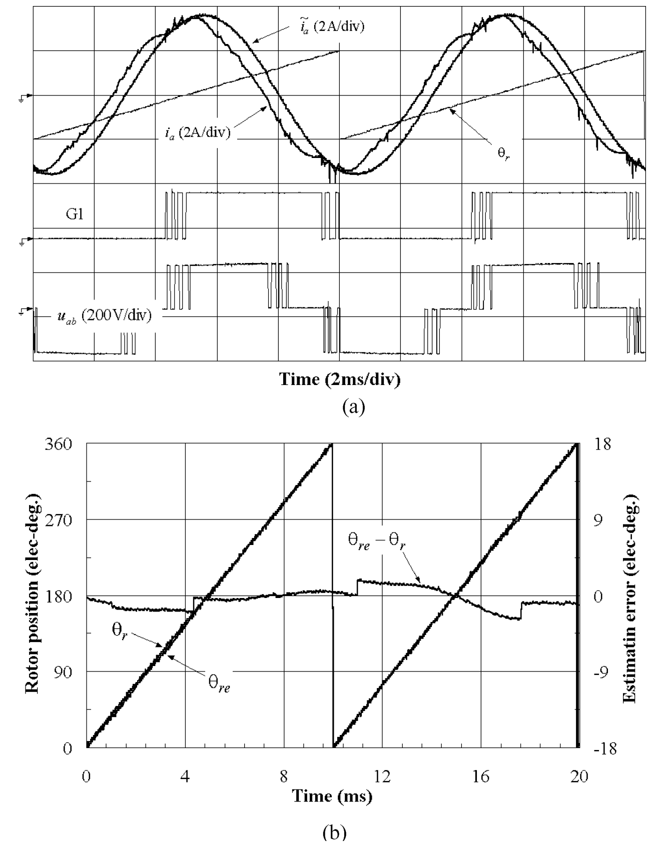

Fig. 13. BLAC operation with flux weakening ($U_{\rm dc} = 200$ V, 2010 r/min, 0.27 N·m). (a) Measured waveforms. (b) Rotor position and error.

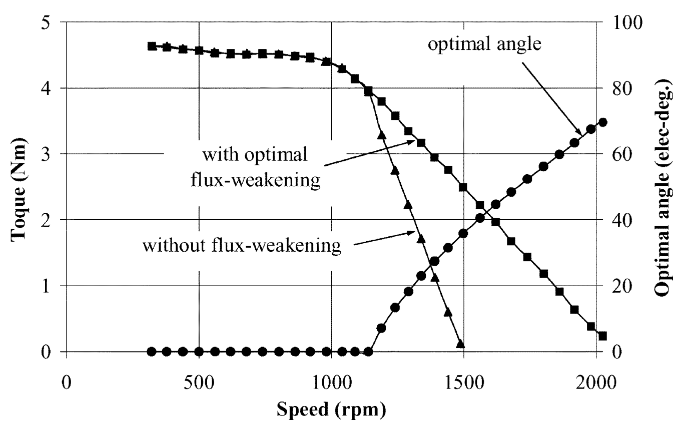

Fig. 14. Torque–speed curves for BLAC operation with and without flux-weakening control, and optimal phase angle between current vector and q axis.

$-I_{\max}$. The q-axis current and the equivalent commutation-advance angle θ_{ad} can then be calculated from (9). This enables a seamless transition between the maximum torque per ampere mode (without flux weakening) and maximum power operating modes (with flux weakening) to be achieved according to the motor speed and parameters.

Third harmonic back-EMF sensorless operation has been assessed both with and without flux weakening, representative waveforms being shown in Figs. 12 and 13, together with the estimated and measured rotor position and rotor position error. Again, good agreement is achieved. Fig. 14 compares the torque–speed characteristics which result both with and without optimal flux-weakening control.

TABLE III
SPECIFICATION AND PARAMETERS OF EXPERIMENTAL MOTOR

Rated DC link voltage (U_{dc}):	200 (V)
Rated power (P_o):	400 (W)
Rated torque (T_e):	4.6 (Nm)
Rated speed (n):	830 (rpm)
Number of pole-pairs (p):	3
Number of slots	18
Phase resistance (R):	3.4 (ohm)
Self-inductance (L):	20.7 (mH)
Mutual-inductance (M):	-2.8 (mH)
Fundamental back-emf (k_{Em1}):	287.3 (mV/(elec-rad/s))
3rd Harmonic back-emf (k_{Em3}):	64.5 (mV/(elec-rad/s))
5th Harmonic back-emf (k_{Em5}):	15.6 (mV/(elec-rad/s))
7th Harmonic back-emf (k_{Em7}):	2.5 (mV/(elec-rad/s))

V. CONCLUSION

The application of third harmonic back-EMF-based sensorless rotor position estimation to both BLDC and BLAC machines has been demonstrated. It caters for phase currents which flow continuously, when the zero crossings of the phase back-EMF waveforms are not detectable. However, as with all EMF-based sensorless methods, an open-loop starting procedure still has to be employed [1]–[3].

APPENDIX

For the specification and parameters of the experimental motor, see Table III.

REFERENCES

[1] K. Iizuka, H. Uzuhashi, M. Kano, T. Endo, and K. Mohri, "Microcomputer control for sensorless brushless motor," *IEEE Trans. Ind. Applicat.*, vol. 21, pp. 595–601, July/Aug. 1985.

[2] S. Ogasawara and H. Akagi, "An approach to position sensorless drive for brushless DC motors," *IEEE Trans. Ind. Applicat.*, vol. 27, pp. 928–933, Sept./Oct. 1991.

[3] M. Jufer and R. Osseni, "Back-emf indirect detection for self-commutation of synchronous motors," in *Proc. 1987 Eur. Conf. Power Electronics and Applications, EPE'87*, 1987, pp. 1125–1129.

[4] R. Wu and G. R. Slemon, "A permanent magnet motor drive without a shaft sensor," *IEEE Trans. Ind. Applicat.*, vol. 27, pp. 1005–1011, Sept./Oct. 1991.

[5] N. Matsui and M. Shigyo, "Brushless DC motor control without position and speed sensors," *IEEE Trans. Ind. Applicat.*, vol. 28, pp. 120–127, Jan./Feb. 1992.

[6] N. Ertugrul and P. Acarnley, "A new algorithm for sensorless operation of permanent magnet motors," *IEEE Trans. Ind. Applicat.*, vol. 30, pp. 126–133, Jan./Feb. 1994.

[7] R. Dhaouadi, N. Mohan, and L. Norum, "Design and implementation of an extended Kalman filter for the state estimation of a permanent magnet synchronous motor," *IEEE Trans. Power Electron.*, vol. 6, pp. 491–497, May 1991.

[8] T. Furuhashi, S. Sangwongwanich, and S. Okuma, "A position and velocity sensorless control of brushless DC motors using an adaptive sliding observer," in *Proc. IEEE IECON'90*, 1990, pp. 1188–1192.

[9] L. Xu and C. Wang, "Implementation and experimental investigation of sensorless control schemes for PMSM in super-high variable speed operation," in *Conf. Rec. IEEE-IAS Annu. Meeting*, 1998, pp. 483–489.

[10] N. Matsui and T. Takeshita, "A novel starting method of sensorless salient-pole brushless motor," in *Conf. Rec. IEEE-IAS Annu. Meeting*, 1994, pp. 386–392.

[11] S. Ostlund and M. Brokemper, "Sensorless rotor-position detection from zero to rated speed for an integrated PM synchronous motor drives," *IEEE Trans. Ind. Applicat.*, vol. 32, pp. 1158–1165, Sept./Oct. 1996.

[12] S. Ogasawara and H. Akagi, "Implementation and position control performance of a position-sensorless IPM motor drive system based on magnetic saliency," in *Conf. Rec. IEEE-IAS Annu. Meeting*, 1997, pp. 464–470.

[13] J. C. Moreira, "Indirect sensing for rotor flux position of permanent magnet AC motors operating over a wide speed range," *IEEE Trans. Ind. Applicat.*, vol. 32, pp. 1394–1401, Nov./Dec. 1996.

[14] F. Profumo, G. Griva, M. Pastorelli, J. C. Moreira, and R. D. Donker, "Universal field oriented controller based on airgap flux sensing via third-harmonic stator voltage," *IEEE Trans. Ind. Applicat.*, vol. 30, pp. 448–455, Mar./Apr. 1994.

[15] A. Testa, A. Consoli, M. Coco, and L. Kreindler, "A new stator voltage third-harmonic based direct field oriented control scheme," in *Conf. Rec. IEEE-IAS Annu. Meeting*, 1994, pp. 608–615.

[16] Z. Q. Zhu, J. D. Ede, and D. Howe, "Design criteria for brushless DC motors for high-speed sensorless operation," *Int. J. Appl. Electromagn. Mech.*, vol. 15, pp. 79–87, 2001/2002.

[17] T. M. Jahns, "Flux-weakening regime operation of an interior permanent magnet synchronous motor drive," *IEEE Trans. Ind. Applicat.*, vol. 23, pp. 681–689, July/Aug. 1987.

[18] S. Morimoto, M. Sanada, and Y. Takeda, "Wide-speed operation of interior permanent magnet synchronous motors with high-performance current regulator," *IEEE Trans. Ind. Applicat.*, vol. 30, pp. 920–926, July/Aug. 1994.

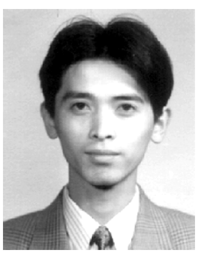

J. X. Shen (M'98–SM'03) was in born in Zhejiang Province, China, in 1969. He received the B.Eng. and M.Eng. degrees from Xi'an Jiaotong University, Xi'an, China, in 1991 and 1994, respectively, and the Ph.D. degree from Zhejiang University, Hangzhou, China, in 1997, all in electrical engineering.

From 1997 to 1999 and from 1999 to 2002, he was a Post-Doctoral Fellow at Nanyang Technological University, Singapore, and the University of Sheffield, Sheffield, UK, respectively. From 2002 to 2004, he was a Research Engineer at IMRA Europe S.A.S., U.K. Research Center, Brighton, U.K. Since 2004, he has been a Professor of Electrical Engineering at Zhejiang University. His current research interests include design and applications of permanent-magnet machines and control.

Z. Q. Zhu (M'90–SM'00) received the B.Eng. and M.Sc. degrees from Zhejiang University, Hangzhou, China, in 1982 and 1984, respectively, and the Ph.D. degree from the University of Sheffield, Sheffield, U.K., in 1991, all in electrical and electronic engineering.

From 1984 to 1988, he lectured in the Department of Electrical Engineering, Zhejiang University. Since 1988, he has been with the University of Sheffield, where he is currently a Professor of Electronic and Electrical Engineering. His current major research interests include applications, control, and design of permanent-magnet machines and drives.

Prof. Zhu is a Chartered Engineer in the U.K. and a Member of the Institution of Electrical Engineers, U.K.

David Howe received the B.Tech. and M.Sc. degrees from the University of Bradford, Bradford, U.K., in 1966 and 1967, respectively, and the Ph.D. degree from the University of Southampton, Southampton, U.K., in 1974, all in electrical power engineering.

He has held academic posts at Brunel and Southampton Universities, and spent a period in industry with NEI Parsons Ltd., working on electromagnetic problems related to turbogenerators. He is currently a Professor of Electrical Engineering at the University of Sheffield, Sheffield, U.K., where he heads the Electrical Machines and Drives Research Group. His research activities span all facets of controlled electrical drive systems, with particular emphasis on permanent-magnet excited machines.

Prof. Howe is a Chartered Engineer in the U.K., and a Fellow of the Institution of Electrical Engineers, U.K., and the Royal Academy of Engineering.